doi:10.1016/j.jmb.2009.07.013 *J. Mol. Biol.* (2009) **xx**, xxx–xxx

JMB

Available online at www.sciencedirect.com

ScienceDirect

ELSEVIER

Reverse Conformational Changes of the Light Chain-Binding Domain of Myosin V and VI Processive Motor Heads during and after Hydrolysis of ATP by Small-Angle X-Ray Solution Scattering

Yasunobu Sugimoto[1]†, Osamu Sato[2]†, Shinya Watanabe[2], Reiko Ikebe[2], Mitsuo Ikebe[2] and Katsuzo Wakabayashi[1]*

[1]*Division of Biophysical Engineering, Graduate School of Engineering Science, Osaka University, Toyonaka, Osaka 560-8531, Japan*

[2]*Department of Physiology, University of Massachusetts Medical School, Worcester, MA 01655-0127, USA*

Received 31 March 2009; received in revised form 4 July 2009; accepted 7 July 2009

We used small-angle X-ray solution scattering (SAXS) technique to investigate the nucleotide-mediated conformational changes of the head domains [subfragment 1 (S1)] of myosin V and VI processive motors that govern their directional preference for motility on actin. Recombinant myosin V-S1 with two IQ motifs (MV-S1IQ2) and myosin VI-S1 (MVI-S1) were engineered from Sf9 cells using a baculovirus expression system. The radii of gyration (R_g) of nucleotide-free MV-S1IQ2 and MVI-S1 were 48.6 and 48.8 Å, respectively. In the presence of ATP, the R_g value of MV-S1IQ2 decreased to 46.7 Å, while that of MVI-S1 increased to 51.7 Å, and the maximum chord length of the molecule decreased by ca 9% for MV-S1IQ2 and increased by ca 6% for MVI-S1. These opposite directional changes were consistent with those occurring in S1s with ADP and Vi or AlF_4^-[2] bound (i.e., in states mimicking the ADP/Pi-bound state of ATP hydrolysis). Binding of AMPPNP induced R_g changes of both constructs similar to those in the presence of ATP, suggesting that the timing of the structural changes for their motion on actin is upon binding of ATP (the pre-hydrolysis state) during the ATPase cycle. Binding of ADP to MV-S1IQ2 and MVI-S1 caused their R_g values to drop below those in the nucleotide-free state. Thus, upon the release of Pi, the reverse conformational change could occur, coupling to drive the directional motion on actin. The amount of R_g change upon the release of Pi was ca 6.4 times greater in MVI-S1 than in MV-S1IQ2, relating to the production of the large stroke of the MVI motor during its translocation on actin. Atomic structural models for these S1s based upon the *ab initio* shape reconstruction from X-ray scattering data were constructed, showing that MVI-S1 has the light-chain-binding domain positioned in the opposite direction to MV-S1IQ2 in both the pre- and post-powerstroke transition. The angular change between the light chain-binding domains of MV-S1IQ2 in the pre- to post-powerstroke transition was ~50°, comparable to that of MII-S1. On the other hand, that of MVI-S1 was ~100° or ~130° much less than the currently postulated changes to allow the maximal stroke size of myosin VI-S1 but still significantly larger than those of other myosins reported so far. The results suggest that some additional alterations or elements are required for MVI-S1 to take maximal working strokes along the actin filament.

Keywords: myosin V-S1; myosin VI-S1; myosin processive motor; light-chain-binding domain; small-angle X-ray scattering

Edited by M. Moody

**Corresponding author.* E-mail address: waka@bpe.es.osaka-u.ac.jp.

† Y.S. and O.S. contributed equally to this work in different parts.

Abbreviations used: SAXS, small-angle X-ray scattering; S1, subfragment 1; LBD, light chain-binding domain; PDB, Protein Data Bank; EGTA, ethylene glycol bis(β-aminoethyl ether)*N*,*N*′-tetraacetic acid; BSA, bovine serum albumin.

Please cite this article as: Sugimoto, Y., et al., Reverse Conformational Changes of the Light Chain-binding Domain of Myosin V and VI Processive Motor Heads During and After a Hydrolysis of ATP..., J Mol Biol (2009), doi:10.1016/j.jmb.2009.07.013

Introduction

It is now evident that myosin constitutes a superfamily of related molecular motors.[1] Newly found myosins are often called "unconventional myosins" because they lack the coiled-coil tail end that forms thick filaments in contrast to myosin II.[2] Nevertheless, unconventional myosins have a conserved motor head domain that permits their function as motor proteins. One of the most important findings is that some unconventional myosins such as myosins V and VI move on actin filaments for long distances without dissociating from them. Since these myosins contain a unique globular tail domain at the distal ends that serves as the docking site for the specific target proteins, which often links myosin to intracellular organelles, it is thought that these myosins function as cargo carriers, thus playing a critical role in cellular trafficking.[1,2]

Myosin V has two heavy chains, each consisting of a motor core domain, a long neck domain with six IQ motifs that bind calmodulin light chains,[3–5] a long coiled-coil domain holding the two heavy chains together to form a stable dimer, and a globular tail. While whether or not the long neck is required for the processive movement of myosin V is controversial,[6–9] myosin V strides along the actin long helical strands in the forward direction [toward the barbed (+) end][3–5,9] with tightly distributed large step sizes of ~36 nm.[8,10–12] On the other hand, it was also found that the two-headed form of myosin VI moves processively on actin filaments with highly variable step sizes between 25 and 36 nm,[13–19] although the two-headed form is not stable and it is anticipated that the dimer formation of myosin VI is regulated in cells.[15,17,20–22] The heavy chain of myosin VI has a unique insertion (insert 2) and one IQ motif, both of which bind calmodulin light chains.[13,23] A critical issue is how myosin VI can move with large steps on actin filaments despite each heavy chain having a shorter neck domain, necessitating substantial structural rearrangement.[13,16,24,25] Another critical issue is how myosin VI moves to the opposite direction [toward the pointed (−) end] on actin filaments,[13,14,17,24,26,27] implying an idea that the cargoes can be transported on actin filaments in both directions in cells. The mechanisms by which processive myosins can perform directional motion along actin filaments with large steps have not been resolved. (Note that processivity is the ability for a two-headed myosin to undergo directional movement along an actin filament without dissociation.)

Recently, the atomic structures of truncated myosin V subfragment 1 (S1)[28,29] and myosin VI-S1[30–32] in the nucleotide-free and transition (or pre-powerstroke) states were partially solved by X-ray crystallography. [The transition state used here is a state in which ATP is hydrolyzed and the products, ADP and Pi (phosphate), are trapped in a molecule, representing the beginning of force-producing movement (powerstroke) once bound to actin.] These results suggested that the light chain-binding domains (LBDs) turn sharply but in opposite directions in the two different myosins during their processive steps. The exact nature and timing, however, of the conformational changes of the motor domain of myosins underlying the opposite directionality of motility on actin filaments during cross-bridge cycling have not yet been determined. Here, we employed small-angle X-ray solution scattering (SAXS) as was previously used to provide evidence for the ATPase cycle-dependent global conformational changes of skeletal muscle myosin S1 under conditions close to physiological,[33–35] to clarify the structural changes of the LBD of these processive myosin motor heads during the ATPase cycle. Our results underscore the role of the conformational changes of the light chain-binding element of these myosin S1 constructs in their directional preference in motility on an actin filament. Based upon the SAXS data, *ab initio* reconstruction was used to derive low-resolution molecular envelopes and, compared with atomic structural models deduced for these constructs, to clarify the extent and nature of orientational changes of their light chain-binding element related to the processive transition.

Results

Myosin V-S1 and VI-S1 constructs

We constructed single-headed truncated myosin V with a short neck domain containing two IQ motifs (MV-S1IQ2 having Met1-Glu822) and single-headed myosin VI containing the motor core domain with a small insertion (insert 1[30]) and the entire neck domain with a unique insertion (insert 2[30]) and a single IQ motif (MVI-S1 having Met1-Glu924)[36] (Fig. 1a) (see Materials and Methods). MV-S1IQ2 and MVI-S1, expressed in Sf9 cells, were purified as described previously,[14] and the purified preparations at low concentrations of Ca^{2+}[37,38] were subjected to gel filtration to remove any aggregates just prior to the X-ray scattering experiments, and only peak fractions were used. Papain-treated chicken skeletal myosin S1 [non-processive myosin II-S1 (MII-S1)] composed of the motor core domain and the neck (tail) domain with both the essential and regulatory light chains was used as a reference for all the experiments (Fig. 1a). Figure 1b shows the molecular components and the relative molecular weights of these constructs as compared to MII-S1 as determined by SDS-PAGE. These results confirmed the components as depicted in Fig. 1a; calmodulin light chains were bound to the IQ motifs and insert 2. The molecular mass of MV-S1IQ2 was ~130 kDa, almost identical with that of MII-S1, and that of MVI-S1 was ~140 kDa, slightly larger than that of MII-S1.

Small-angle X-ray solution scattering

A series of SAXS measurements on nucleotide-free and nucleotide-bound myosin complexes were carried out with a focusing small-angle diffractometer[39,40]

Please cite this article as: Sugimoto, Y., et al., Reverse Conformational Changes of the Light Chain-binding Domain of Myosin V and VI Processive Motor Heads During and After a Hydrolysis of ATP..., J Mol Biol (2009), doi:10.1016/j.jmb.2009.07.013

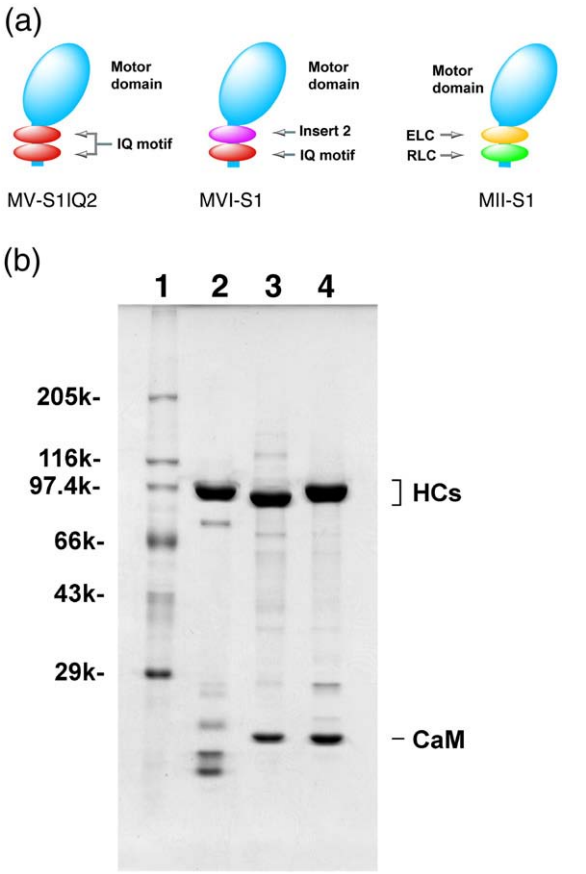

Fig. 1. Structure of myosin S1 constructs. (a) Schematic drawing of the myosin V-S1IQ2 and myosin VI-S1 constructs and skeletal myosin II-S1 used in the experiments. The MV-S1IO2 construct (Met1-Glu822) contains a motor core domain and two IQ motifs. The MVI-S1 construct (Met1-Glu924) consists of a motor core domain, insert 2, and a single IQ motif. MII-S1 has a motor core domain, a regulatory light chain (RLC), and an essential light chain (ELC). (b) SDS-PAGE patterns of the purified myosin S1 constructs. Shown are molecular mass markers (lane 1), MII-S1 (chicken skeletal myosin S1) (lane 2), MV-S1IQ2 (lane 3), and MVI-S1 (lane 4). The molecular masses (in daltons) of the marker proteins were indicated to the left of the panel. The apparent molecular mass of the heavy chain of each myosin S1 construct was consistent with the expected molecular masses (ca 100, 95, and 107 kDa for HCs of MII-S1, MV-S1IQ2, and MVI-S1, respectively). Calmodulin bands were seen in the purified MV-S1IQ2 and MVI-S1 constructs. HCs and CaM in the right of the panel represent heavy chains and calmodulin, respectively.

using synchrotron X-rays from the Photon Factory storage ring and a linear position-sensitive proportional detector at camera lengths of 2.42 and 1.02 m (see Materials and Methods). SAXS measurements were done at 20 °C on each myosin class construct in the presence of 2 mM MgATP at pH 7.5 immediately after mixing with ATP in short exposure times less than 90 s to minimize the radiation damage to the samples. The temperature and pH value were fixed so as to maximize the population of the predominant species of these S1s in the presence of ATP[41] (see below). Experiments in other nucleotide-bound states were also performed at the same temperature and pH. Figure 2 shows examples of Guinier plots of the SAXS data ($\ln[I(Q,c)]$ *versus* Q^2 plot[42]) from two processive myosin S1 samples, where $I(Q,c)$ is the net scattered X-ray intensities at protein concentration, c, and Q is the scattering vector ($4\pi\sin\theta/\lambda$). All plots gave a straight line with no significant upturn in the small-angle region $Q^2 \leq 8.0\times10^{-4}$ Å^{-2} showing little aggregation of the molecules in solution.

Figure 3 shows the inverse zero-angle intensity [$c/I(0,c)$] *versus* c plot, where $I(0,c)$ was obtained by the extrapolation of the straight line in the small-angle region (see below) in the Guinier plot of $I(Q,c)$ to $Q=0$ for c of each sample under the same experimental conditions. The plots exhibited linear concentration dependence for each myosin sample with a very moderate slope (nearly zero values of the second virial coefficient). Extrapolation of $c/I(0,c)$ to $c=0$ enables one to derive the molecular mass[42] of the two constructs relative to the mass of MII-S1 (130 kDa) by assuming the same value of partial specific volume for these proteins (Table 1). The molecular masses of the MV-S1IQ2 and MVI-S1 constructs derived were almost identical with the values examined from the SDS-PAGE (Fig. 1b).

Changes in radius of gyration

The apparent radius of gyration, $R_g(c)$, was calculated from the slope of the inner part (2.50×10^{-4} Å$^{-2} \leq Q^2 \leq 8.00\times10^{-4}$ Å^{-2}) of the Guinier plots in Fig. 2. The radius of gyration denotes the root-mean-square distances at all elemental scattering volumes from the center of gravity of electron densities of the molecule. Figure 4 shows the squared $R_g(c)$ values of the MV-S1IQ2 (Fig. 4a) and MVI-S1 (Fig. 4b) constructs as a function of protein concentrations (c) together with those of MII-S1 (Fig. 4c). (The squared R_g *versus* c plot was used because the slope of the Guinier plot in the small-angle limit is

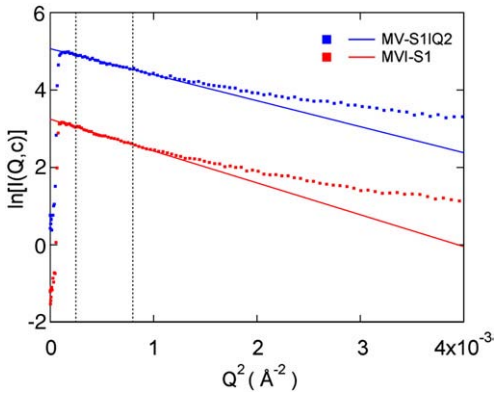

Fig. 2. SAXS curves of MV-S1IQ2 and MVI-S1 samples on a Guinier plot ($\ln[I(Q,c)]-Q^2$). The straight lines represent extrapolated Guinier fits. The fitting ranges of the straight lines are indicated by vertical lines in which the Guinier criterion ($QR_g=1$) is included. For clarity, the curves are shifted by an arbitrary unit on the $\ln[I(Q,c)]$ axis. The scattering data in this example were measured at 5 mg/ml protein concentrations.

Please cite this article as: Sugimoto, Y., et al., Reverse Conformational Changes of the Light Chain-binding Domain of Myosin V and VI Processive Motor Heads During and After a Hydrolysis of ATP..., J Mol Biol (2009), doi:10.1016/j.jmb.2009.07.013

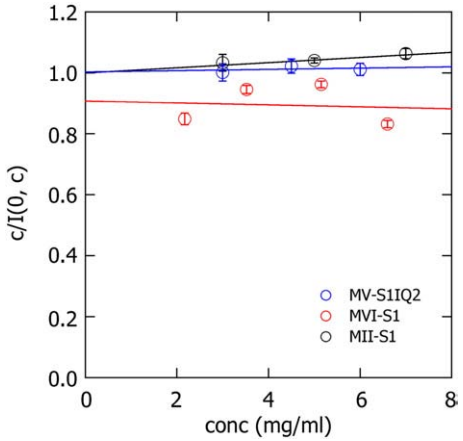

Fig. 3. Protein concentration (c) dependence of the normalized zero-angle intensity [$c/I(0,c)$]. $I(0,c)$ was obtained by extrapolation of the Guinier plot of $I(Q,c)$ data to $Q=0$. Extrapolation of this plot to $c=0$ by means of a variance-weighted least-squares fit to the data points yields the molecular mass of proteins (see Table 1). Blue circles, MV-S1IQ2; red circles, MVI-S1; black circles, MII-S1. Vertical bars are associated SDs.

$-R_g^2/3$ in which the squared R_g is dependent upon c.[42]) The plots had a slightly positive slope with increasing c except for nucleotide-free MVI-S1, indicative of small interference effects due to protein-protein attractive forces at short distances of approach.

True values, extrapolated to $c=0$, are given as R_g in Table 1. R_g of the nucleotide-free MII-S1 was ca 47.8 Å and decreased by ca 2 Å in the presence of ATP, the values of which are comparable to those reported previously.[33–35] The change in R_g of the MV-S1IQ2 construct upon the addition of ATP was nearly the same as MII-S1 in both proportion and direction; that is, R_g of the nucleotide-free construct was ca 48.6 Å and decreased by ca 2 Å in ATP solution, indicating

Table 1. The radius of gyration (R_g), the maximum chord length (D_{max}), and the molecular mass of the MV-S1IQ2 and MVI-S1 samples compared with those of the MII-S1 sample

Sample	R_g (Å)	D_{max} (Å)	Molecular mass (kDa)
MII-S1			
No nucleotide	47.8±0.05	160	130±5
+ATP	45.6±0.04	150	
MV-S1IQ2			
No nucleotide	48.6±0.26	160	130±7
+ATP	46.8±0.20	145	
+ADP	47.5±0.46	150	
+AMPPNP	46.7±0.50	150	
MVI-S1			
No nucleotide	48.8±0.06	175	144±5
+ATP	51.7±0.09	185	
+ADP	47.2±1.01	170	
+AMPPNP	51.1±0.77	180	
+ADP.AlF_4	51.5±0.76	185	

The R_g at $c=0$ is listed. The R_g and molecular mass values are shown with associated SDs. The D_{max} values were determined with an uncertainty of ±5 nm.

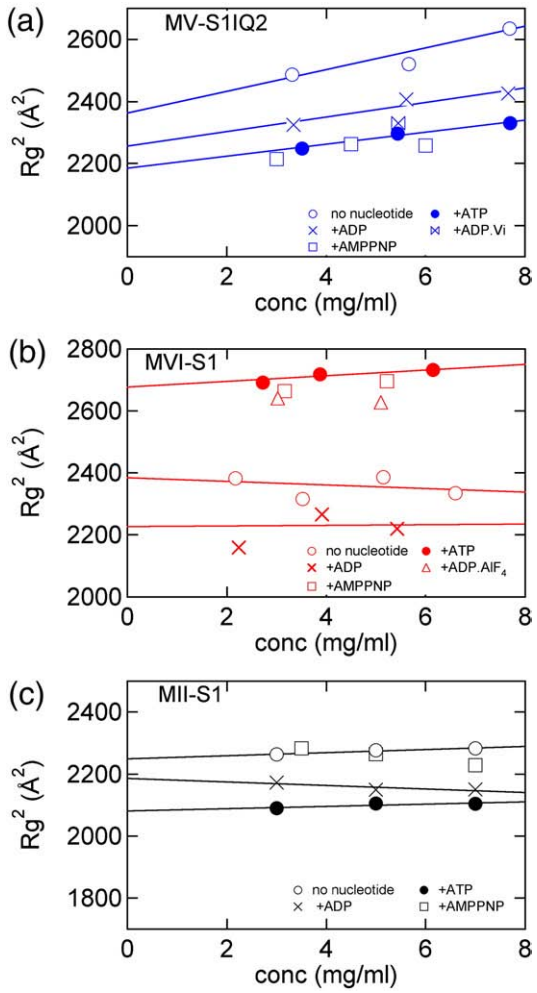

Fig. 4. Protein concentration dependence of the squared apparent radius of gyration (R_g^2) of various S1 samples derived from the Guinier plot of $I(Q,c)$ data. (a) MV-S1IQ2 construct, (b) MVI-S1 construct, and (c) MII-S1 (as a reference). The open and filled circles denote the values of myosin S1 samples in the absence (no nucleotide) and presence of MgATP (+ATP), respectively. The crosses denote the values of the samples with the addition of MgADP (+ADP), and the squares denote those of the samples upon the addition of MgAMPPNP (+AMPPNP). In (a), the double triangle denotes the value of MV-S1IQ2-bound MgADP and Vi (+ADP.Vi). In (b), the triangles denote the value of MVI-S1-bound MgADP and AlF_4^{-2} (+ADP.AlF_4). The R_g values at $c=0$ were determined by means of the variance-weighted least-squares fit to the data points and are listed in Table 1.

that the MV-S1IQ2 molecule became more compact or rounded as was revealed with MII-S1 (see below) where the overall size of the molecule is the major determinant of the R_g.[33–35] In contrast, R_g of the MVI-S1 construct changed in the opposite way to that of MII-S1; that is, R_g of the nucleotide-free MVI-S1 was ca 48.8 Å, slightly larger than that of MII-S1, and increased by ca 3 Å in ATP solution, indicating that the MVI-S1 molecule became more extended or lengthened upon the addition of ATP (see below). When MV-S1IQ2 and MVI-S1 constructs bound MgADP plus Vi (vanadate) or AlF_4^{-2} (aluminum fluoride)

Please cite this article as: Sugimoto, Y., et al., Reverse Conformational Changes of the Light Chain-binding Domain of Myosin V and VI Processive Motor Heads During and After a Hydrolysis of ATP..., J Mol Biol (2009), doi:10.1016/j.jmb.2009.07.013

[where Vi and AlF_4^{-2} are known to be analogs of phosphate (Pi)[34,43]], they underwent a change in R_g similar to that in ATP solution (see Fig. 4 and Table 1), implying that these two constructs in the presence of ATP remained trapped in an ADP/Pi-bound state.

It is worthwhile mentioning that both constructs underwent a change in R_g upon the addition of MgAMPPNP (adenylylimidodiphosphate, a nonhydrolyzable analog of ATP[43]) similar to that in ATP solution, while binding of AMPPNP did not cause such an appreciable change for MII-S1 (see Fig. 4 and Table 1). This finding suggests that molecular changes of these processive myosin S1s in the presence of ATP occur in the pre-hydrolysis step (S1*.ATP),[44] leading to a "primed" conformation of the predominant intermediate, S1**.ADP.Pi (where asterisks on S1 denote the extent of enhancement of fluorescence intensity, indicative of local changes of nucleotide binding motif). Note that the term "primed" dictates the orientation of the LBD of S1 found in the ADP.Pi-bound state (see below). The addition of MgADP to the nucleotide-free molecules caused the decrease in R_g by ca 1 Å for MV-S1IQ2 similar to MII-S1 and by ca 1.6 Å for MVI-S1 (Fig. 4 and Table 1). These results suggest that the release of Pi from the S1**.ADP.Pi state causes a reversal (re-priming) of the conformational change in these S1s. Following the release of ADP, their conformations return to the nucleotide-free state with a slight increase in R_g (Table 1 and see Fig. 9).

Changes of pair-distance distribution functions

The SAXS intensity data have been obtained for a number of concentrations to enable the extrapolation for infinite dilution [$I(Q,0)$] for all samples in the range less than $Q \sim 0.07$ Å^{-1}, and the average profile of the extrapolated values have been calculated. The high-Q SAXS intensity data (beyond $Q \sim 0.07$ Å^{-1}), which were obtained at high protein concentrations with the short camera length, were spliced to the low-Q data by a least-squares fitting procedure by using the intensity data of 0.05 Å$^{-1} \le Q \le 0.09$ Å^{-1}. Figure 5 shows the pair-distance distribution function, $p(r)$,[42] calculated by an indirect Fourier transformation of the $I(Q,0)$ data[42,45] in the range 0.016 Å$^{-1} \le Q \le 0.240$ Å^{-1} from each sample in comparison between the nucleotide-free state and in the presence of ATP. The $p(r)$ denotes the histogram of the pair distances, r, between two volume elements within the molecule. The r-intercept of $p(r)$ gives the maximum chord length, D_{max}, of the molecule. In Fig. 5c, the $p(r)$ curve of MII-S1 in the presence of ATP intersects the nucleotide-free curve around $r \sim 100$ Å, and there is a higher frequency of pair distances from $r \sim 35$ Å to 100 Å and a lower frequency of them beyond $r \sim 100$ Å, resulting in D_{max} being shorter by ca 10 Å in ATP solution than in the nucleotide-free state ($D_{max} \sim 160$ Å) as was reported previously.[33,34] In Fig. 5a, the $p(r)$ curve of MV-S1IQ2 in the presence of ATP showed a change similar to that observed for MII-S1. D_{max} of the nucleotide-free MV-S1IQ2 was ca 160 Å, which was almost the same as that of MII-S1.

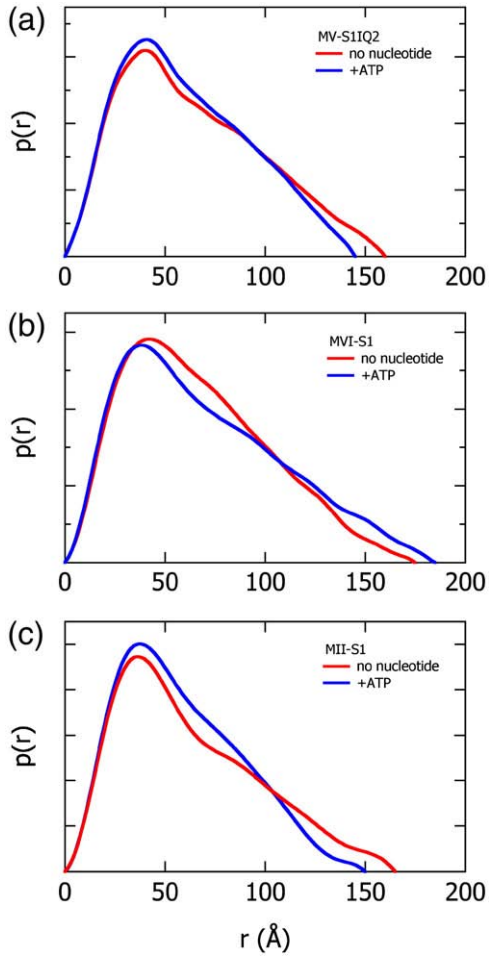

Fig. 5. Pair-distance distribution functions, $p(r)$, of three myosin S1 samples derived from an indirect Fourier transformation of $I(Q,0)$ data. (a) MV-S1IQ2 construct, (b) MVI-S1 construct, and (c) MII-S1. The red and blue curves denote the $p(r)$ function in the absence (no nucleotide) and presence of MgATP (+ATP), respectively. Each $p(r)$ curve is normalized in its integrated value. The maximum chord length, D_{max}, of the molecule is defined as the distance at which the $p(r)$ eventually drops to zero, that is, the r-intercept (see Table 1).

D_{max} was reduced by ca 15 Å (ca 9%) in ATP solution. In contrast, the $p(r)$ curve of MVI-S1 in the presence of ATP showed a lower frequency of pair distances between the peak and the intersecting point with the nucleotide-free curve (around $r \sim 100$ Å) and a higher frequency of them beyond the intersecting point, resulting in D_{max} of the MVI-S1 molecule being longer by ca 10 Å (ca 6%). D_{max} of the nucleotide-free MVI-S1 was ca 175 Å, which was greater by ~15 Å than that of MV-S1IO2 or MII-S1 (Fig. 5b). The larger D_{max} of this construct may be due to the presence of the extra residues (~85 residues) following the IQ motif (see Materials and Methods). The peak position ($r \sim 35$ Å) of the nucleotide-free curve was almost the same as that of the MV-S1IQ2 curve or the MII-S1 curve, but the peak shifted slightly toward low r in ATP solution, being close to that of the MII-S1 curve. The D_{max} values are summarized in Table 1. The R_g values

Please cite this article as: Sugimoto, Y., et al., Reverse Conformational Changes of the Light Chain-binding Domain of Myosin V and VI Processive Motor Heads During and After a Hydrolysis of ATP..., J Mol Biol (2009), doi:10.1016/j.jmb.2009.07.013

calculated as the second moment of these $p(r)$ functions[42] agreed within experimental errors with those obtained from Guinier analysis of the SAXS data. The different profiles of $p(r)$ in the absence and presence of ATP reflect the alterations in molecular shape of these S1 molecules.

Ab initio shape reconstruction of the MV-S1IQ2 and MVI-S1 constructs in the nucleotide-free state and in the presence of ATP

We modeled S1 shape changes of these two constructs with the use of the *ab initio* shape-prediction program DAMMIN that has been successfully employed to model the conformation of globular proteins in solution[46,47] (see Materials and Methods). Simulations were conducted under the assumption of a single average conformation of S1 molecules in solution (see Discussion). A protein shape was first expressed by a face-centered cubic spherical ball-filling model in a volume that is confined by D_{max} of $p(r)$ functions and was then optimized with a compactness criterion by removing and/or adding balls in appropriate places. A simulated annealing procedure was used so as to best fit the observed X-ray scattering intensity curves. The final models with a least residual (R-factor) (see Materials and Methods) were obtained by the refinement calculation from the average structure of 10 possible reconstructions that were derived in the independent repeat runs. Application of this shape-prediction algorithm to the X-ray scattering intensity data of MII-S1 has yielded a shape, consistent with the crystallographically determined structure[47] (also Sugimoto *et al.*, unpublished work). The reconstituted bead models are described by the molecular envelope profile maps.

Figure 6a–d shows the best-fit *ab initio* molecular envelopes for the two constructs in stereo views in the nucleotide-free state and in the presence of ATP. As expected, the shape of the MV-S1IQ2 construct changed in ATP solution into a more rounded form like a camel's humped back (Fig. 6b) as compared to that for the nucleotide-free construct (Fig. 6a) where the shape appeared to be rather elongated. In contrast, the MVI-S1 construct appeared to have a sharply bent shape in the nucleotide-free state (Fig. 6c), and in the presence of ATP, it became a more elongated form with a twist around the long axis of the molecule (like a "turned-on letter S") (Fig. 6d).

Construction of atomic structural models for the MV-S1IQ2 and MVI-S1 constructs in the nucleotide-free state and in the presence of ATP

In order to clarify the extent of motions or the conformational changes that account for the shape changes of these constructs in the nucleotide-free state and in the presence of ATP, we attempted to construct the atomic structural models for the MV-S1IQ2 and MVI-S1 constructs by using existing crystal structure data. In modeling the MV-S1IQ2 construct in the nucleotide-free state, the crystal structure of the LBD portion of MV-S1 [Protein Data Bank (PDB) ID: 2IX7[48]] with calmodulin bound to the two IQ motifs was combined to the crystal structure consisting of the motor core domain and an IQ1 portion (i.e., MV-S1IQ1 in our terms) (PBD ID: IOE9[28]) with a PyMOL molecular graphic system[49] (see Materials and Methods). The matching between the atomic structural model constructed and the SAXS-derived molecular envelope was performed by the program (SUPCOMB) of Kozin and Svergun.[50] When the motor core domain of the atomic structural model was aligned optimally to one end of the SAXS molecular envelope of MV-S1IQ2, the LBD of the atomic structural model held mostly in place of the rest of the SAXS molecular envelope without a further alteration in the orientation of the LBD (Fig. 7a). For modeling the structure in the presence of ATP, the same atomic structural model as above was used, because crystal structures mimicking the ADP/Pi-bound state have not been determined. The motor core domain of the atomic structural model was fitted to one end of the SAXS-derived molecular envelope obtained in ATP solution and then the LBD was pivoted around Gly686, which locates near an SH-helix of the converter, as a fulcrum (see Fig. 7c) to fit to the rest of the SAXS molecular envelope. Rotation, tilting, and twisting of the functional domains were involved, and the converter itself was rotated as a rigid body, rectifying the LBD orientation. The orientation of the lever arm was varied by changing angles of two differently directed tilts with steps of 10°, and the best-fit orientation was searched by calculating minimal R-factor between the calculated and observed intensity data. The final optimal model was determined by further examining the goodness of fit with the SAXS molecular envelope and the overall agreement between the calculated and observed intensity profiles. There were two types of the optimal atomic structural models that satisfied coordinately the selection criteria as mentioned above; one type is that orientation change of the LBD is caused mainly by its longitudinal component of the force-producing throw and the other type is that the change of LBD orientation is caused dominantly by the transversal component of it. We adopted the model with a longitudinal component, which could operate as the major component of the force-producing throw of the processive motors on actin.

The adopted atomic structural model in ATP solution was obtained by turning the LBD by ~50° (Fig. 7b). In this model, the cone-shaped portion connecting the motor core domain and the LBD portion is likely to form "the camel's hump". In the nucleotide-free state, the molecule had a moderate bend between the motor core domain and the LBD (the angle between them was ~140°), and in ATP solution, it had a doglegged form with a sharp bend of the LBD (the corresponding angle was ~100°). Figure 7c compares the atomic structural models in the nucleotide-free state and in the presence of ATP as a net change in the ATPase cycle when the motor core domains were superimposed with each other. The angular change between the α-helical backbones of the LBD in both models was about 50° with an uncertainty

Please cite this article as: Sugimoto, Y., et al., Reverse Conformational Changes of the Light Chain-binding Domain of Myosin V and VI Processive Motor Heads During and After a Hydrolysis of ATP..., J Mol Biol (2009), doi:10.1016/j.jmb.2009.07.013

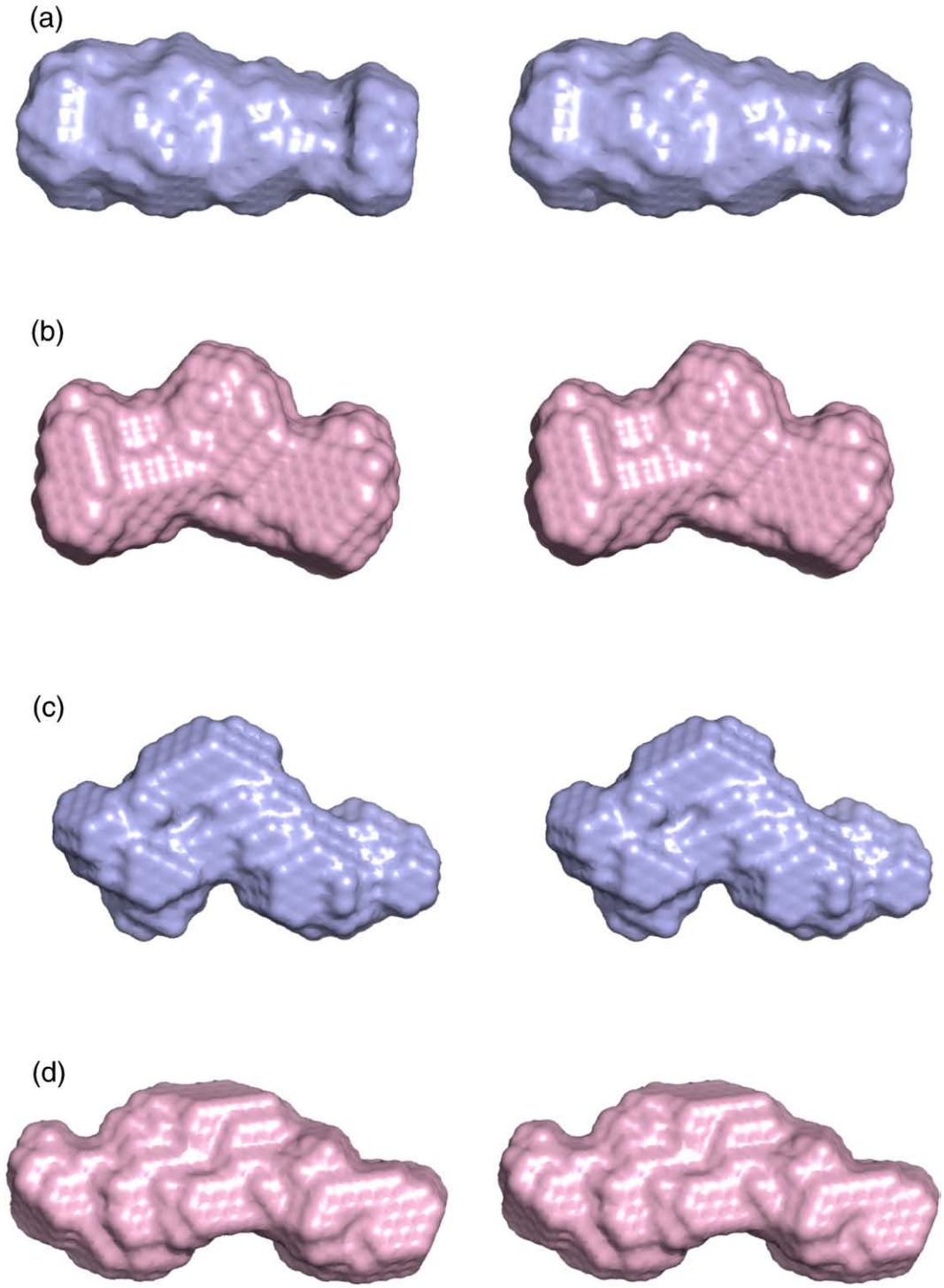

Fig. 6. ATP-induced changes in molecular shape of the MV-S1IQ2 and MVI-S1 constructs. The general shapes of both constructs were derived by using an *ab initio* shape prediction program (DAMMIN). They are shown in the stereo view. (a) and (b) are the molecular shapes of MV-S1IQ2 in the nucleotide-free state and in the presence of MgATP, respectively, and (c) and (d) are those of MVI-S1 in the nucleotide-free state and in the presence of MgATP, respectively.

of ±10°, which was smaller than that (~70°) estimated by single-molecule fluorescence polarization[11] but was comparable to that in MII-S1 as determined by previous SAXS studies[33–35] and the present work.

Similarly, the atomic structural model for the MVI-S1 construct in the nucleotide-free state was constructed by using the partial crystal structure of MVI-S1IQ1 (PDB ID: 2BKI[28]) (containing the motor core domain and insert 2 plus an IQ motif) and the LBD crystal structure of MV-S1 (PDB ID: 2IX7) since we do not have the crystal structure with the LBD of MVI-S1. The two crystal structures were aligned and then combined with each other to obtain a complete model of the atomic structure (see Materials and Methods). The

Please cite this article as: Sugimoto, Y., et al., Reverse Conformational Changes of the Light Chain-binding Domain of Myosin V and VI Processive Motor Heads During and After a Hydrolysis of ATP..., J Mol Biol (2009), doi:10.1016/j.jmb.2009.07.013

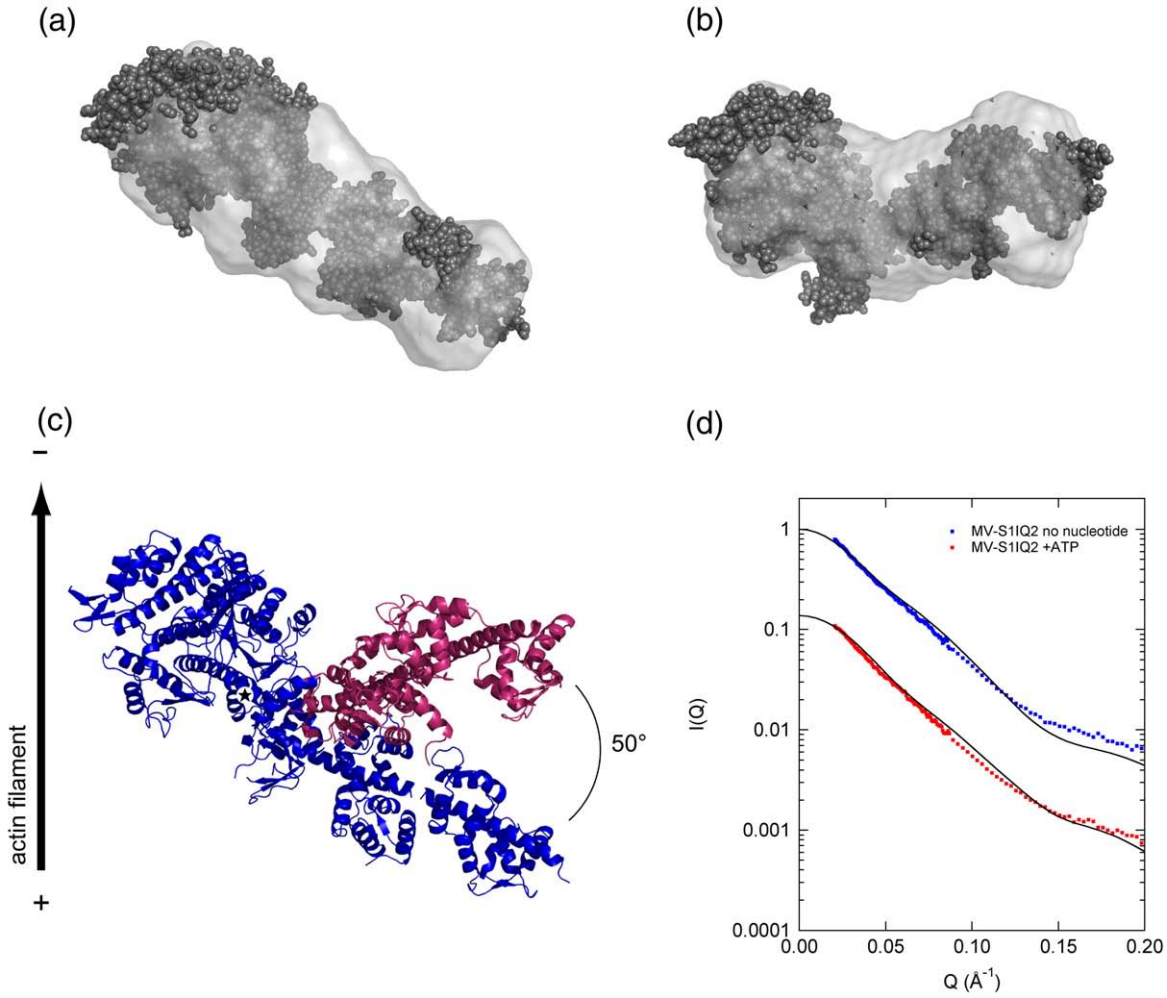

Fig. 7. Matching of the atomic structural model for the MV-S1IQ2 construct into the SAXS-derived shape envelope. (a) In the nucleotide-free state and (b) in the presence of MgATP. The atomic structural model consisting of the partial crystal structures of a motor core domain (PDB ID: 1OE9) and an LBD domain (PDB ID: 2IX7) is represented with a space-filled model. (c) A comparison of the crystal structural models in the nucleotide-free state (blue) and in MgATP solution (red) with their motor core domains superimposed, represented with a ribbon model. The pivot point (Gly686) of the LBD is marked by a star in (c). For a detailed explanation, see the text. All S1 models are aligned perpendicularly to the actin filament as shown in (c), pointing toward the minus end. (d) Comparisons of the scattering intensities calculated from the models (continuous curves) and the observed intensities (dots) of the MV-S1IQ2 construct in the nucleotide-free state (no nucleotide) (blue) and in MgATP solution (+ATP) (red). The two curves are shifted by an arbitrary unit on the ln[$I(Q)$] axis.

model obtained had a high degree of bending of the LBD, which was consistent with the model derived from the crystal data by Ménétrey *et al.*[30,31] but was largely different from the SAXS-derived molecular envelope in the bending magnitude of the LBD. For an optimal matching with the SAXS envelope in the nucleotide-free state, the orientation between the motor core domain and the LBD in the atomic structural model was altered in a similar way as in the case of MV-S1IQ2 by rotating the LBD around Gly704, which resides in an N-terminal side to the converter region (see Fig. 8c). The optimal model was searched and determined with the same procedures as was done in MV-S1IQ2 in ATP. There were two types of the optimal atomic structural models that satisfied coordinately the selection criteria as mentioned above similarly to the case of MV-S1IQ2 in ATP, and the appropriate model was selected as above. It was obtained by unbending the LBD relative to the motor core domain by ~50° with an uncertainty of ±10° (Fig. 8a and c). The altered model appears to fit well with the SAXS-derived molecular envelope in the nucleotide-free state.

An atomic structural model for MVI-S1 in the presence of ATP was constructed by using the partial crystal structure of MVI-S1 (PDB ID: 2V26[31]) and the LBD crystal structure of MV-S1 (2IX7). The crystal structure of 2V26 has the motor core domain including the residues until the proximal helix of insert 2 and with ADP and Vi bound to the nucleotide binding sites, which has a dramatic alteration in the converter position and in the orientation of the proximal helix of insert 2 compared to MV-S1IQ2 or MII-S1; it mimics an ADP/Pi-bound structure and the kink in the insert 2 helix is present.[31] This atomic structural model seemed to fit well with the SAXS

Please cite this article as: Sugimoto, Y., et al., Reverse Conformational Changes of the Light Chain-binding Domain of Myosin V and VI Processive Motor Heads During and After a Hydrolysis of ATP..., J Mol Biol (2009), doi:10.1016/j.jmb.2009.07.013

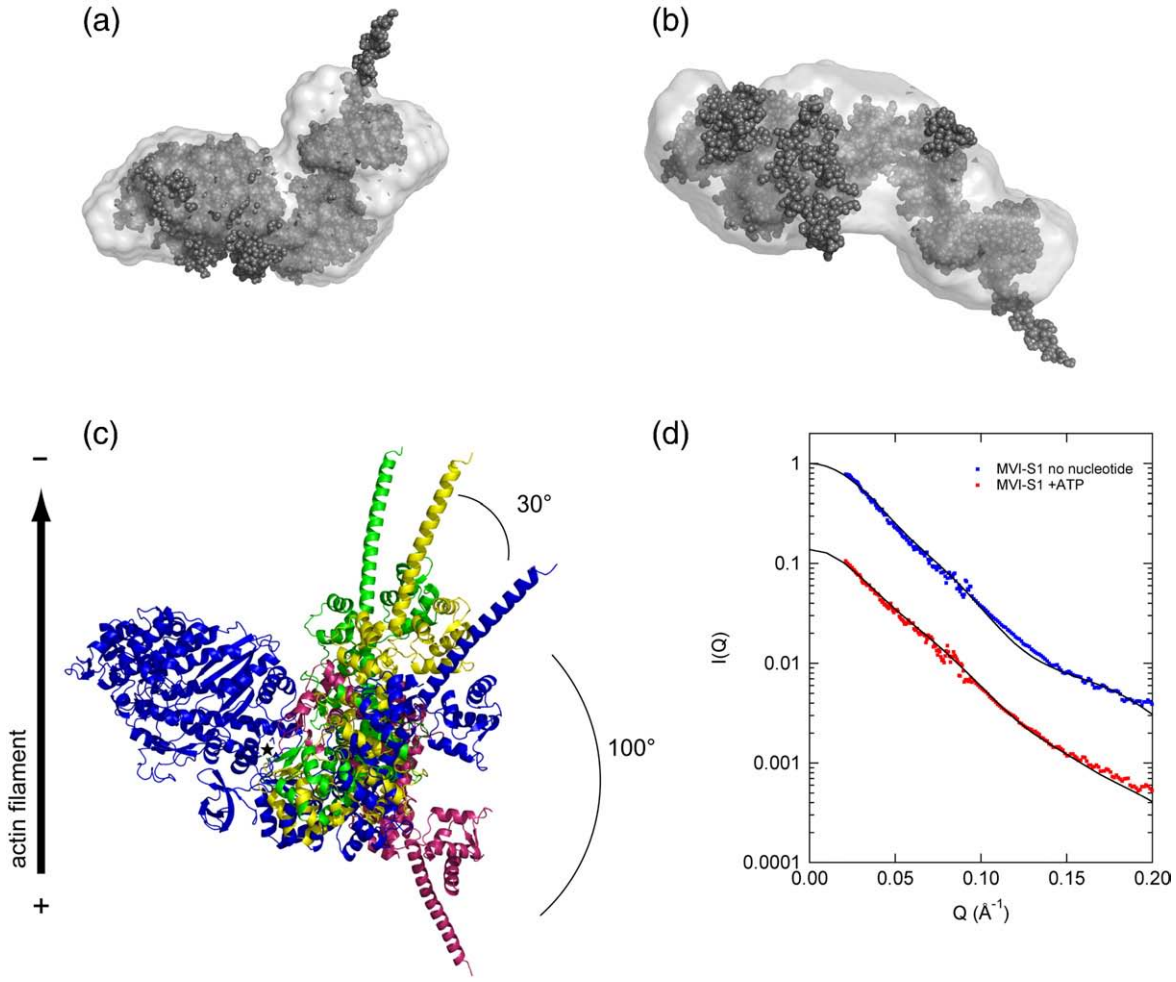

Fig. 8. Matching of the atomic structural model for the MVI-S1 construct into the SAXS-derived shape envelope. (a) In the nucleotide-free state and (b) in the presence of MgATP. The atomic structural model in the nucleotide-free state consists of the partial crystal structures of MVI-S1IQ1 (PDB ID: 2BKI) and the LBD domain of MV (PDB ID: 2IX7), and the model in MgATP solution consists of the partial crystal structure of the motor core domain (PDB ID: 2V26) and the LBD domain of MV (PDB ID: 2IX7). They are represented with a space-filled model. (c) A comparison of the crystal structural models in the nucleotide-free state (blue) and in MgATP solution (red) with their motor core domains superimposed. For a comparison, the model consisting of the partial crystal structure (2BKI) plus the LBD (green) and the optimal model of this S1 in the ADP-bound state (yellow) are shown together. The pivot point (Gly704) of the LBD is marked by a star in (c). For a detailed explanation, see the text. The alignment of S1s is the same as that in Fig. 7. (d) Comparisons of the scattering intensities calculated from the models (continuous curves) and the observed intensities (dots) of the MVI-S1 construct in the nucleotide-free state (no nucleotide) (blue) and in MgATP solution (+ATP) (red). The two curves are shifted by arbitrary units on the ln[$I(Q)$] axis.

molecular envelope in the presence of ATP without a further alteration (Fig. 8b). Figure 8c compares the atomic structural models in the nucleotide-free state and in the presence of ATP as a net change with their motor core domains superimposed as in the case of MV-S1IQ2. [For a comparison, the model consisting of the partial crystal structure (2BKI) plus the LBD and the optimal model of this S1 in the ADP-bound state (see below) are shown together.] The angular change between the α-helical backbones of the LBD in both models was about 100°, Figures 7d and 8d compare the intensity data in the Q-range where the "shape" scattering dominates,[51] calculated from the respective optimal models and the observed data of MV-S1IQ2 and MVI-S1, in the nucleotide-free state and in ATP solution, respectively, showing a reasonable agreement between them in each case; the intensity *R*-factor (see Materials and Methods) was 0.0085 in the nucleotide-free state and 0.0077 in ATP solution for MV-S1IQ2 and 0.0074 in the nucleotide-free state and 0.0064 in ATP solution for MVI-S1.

Note that in the atomic structural models of MVI-S1 (Fig. 8a and b), about 30 residues of the α-helical backbone of the LBD lie out of the SAXS-derived molecular envelope. The length of the LBD of our construct used is longer by ~60 residues than that of the atomic structural model (see Materials and Methods). Thus, an ~90-residue length portion of the LBD may lie outside of the molecular envelope. Since such a long portion was not seen in the SAXS molecular envelope, it might be folded back within the envelope and fill up the space in the tail portion in

Please cite this article as: Sugimoto, Y., et al., Reverse Conformational Changes of the Light Chain-binding Domain of Myosin V and VI Processive Motor Heads During and After a Hydrolysis of ATP..., J Mol Biol (2009), doi:10.1016/j.jmb.2009.07.013

the low Ca^{2+} state as recently suggested by Spink *et al.*[52] Alternatively, highly mobile segment beyond the IQ motif[18,53] would be filtered out in the shape determination and averaging process.

We did not attempt to refine further the obtained atomic structural models for both S1s to make a better fit to the observed intensity data because of the lack of information concerning detailed structural alterations within the molecules.

MV alters the molecular shape of the S1 portion into a more bent form during hydrolysis of ATP in the same manner as S1 of MII does,[33–35] while MVI changes the shape of S1 into a more elongated form in the presence of ATP. The latter observation is consistent with electron microscopic images of single particles showing that the molecules in ATP solution are relatively straight while apo molecules have a bent or hooked appearance.[15,17,21] The primed conformations of these S1s in ATP solution are re-primed upon the release of Pi or ADP to perform a processive transition.

Discussion

Conformational changes of MV-S1IQ2 and MVI-S1 during and after hydrolysis of ATP

It is known that ATP bound to conventional myosin rapidly undergoes hydrolysis via an isomerization after binding to form a myosin/ADP/Pi intermediate (a key intermediate state).[44] The X-ray scattering intensity profiles from MV-S1IQ2 and MVI-S1 in the presence of ATP were very similar to their respective curves from the ADP and Vi- or AlF_4^-[2]-bound forms. This indicates that in these processive myosins in the absence of actin, ADP and Pi predominantly remain trapped in the nucleotide binding site during the steady-state of ATP hydrolysis, similarly to MII, with their LBDs in a "primed" conformation, representing a transition or pre-powerstroke state. This is consistent with the results of enzyme kinetic analysis, suggesting that the rate-limiting step of the ATP hydrolysis cycle for these myosins is the Pi-off step in the absence of actin due to slow release of the products. In the presence of actin, however, it is thought that the ADP/Pi-bound form of these myosins is rapidly converted to the ADP-bound form to produce a strong actin-bound ADP state as a stable intermediate of the overall ATPase cycle, allowing processivity.[54–57] Such a state is thought to be necessary to produce a highly strain-sensitive ADP release.[58]

Our SAXS data showed that the R_g values of MVI-S1 upon ATP binding increased whereas those for MV-S1IQ2 or MII-S1 decreased, suggesting that the primed conformation of MVI-S1 is a more elongated form in contrast to MV-S1IQ2 in which it is more compact. ADP binding to MV-S1IQ2 and MVI-S1 caused a decrease of R_g to values below those found in the nucleotide-free state (see Fig. 4 and Table 1). This indicates that the reversal of the primed conformations (force-producing conformational change) occurs upon the release of Pi from an S1**.ADP.Pi state in both constructs. The SAXS experiments with AMPPNP suggest that a primed conformation in the transition state is already prepared during the isomerization step (S1*.ATP state) just after ATP binding of ATPase cycle; that is, a rapid rearrangement in the structure could be produced following the detachment from actin and return to the pre-powerstroke conformation. This timing is similar to a myosin Va[59] and a kinesin motor,[60] whereas the binding of AMPPNP does not cause any appreciable change in R_g for non-processive MII-S1 (see Fig. 2). A conflicting model of these motors by binding of AMPPNP has been proposed on the basis of crystal structures that reported that MVI-S1 underwent little change in conformation upon binding of ADP and BeF_3^-[X] (another Pi analog[43]) which is supposed to mimic the same state as the AMPPNP state.[32] It is known that a fluoroberyllate compound is a mixture of two stereochemically different species, and both species may be bound. Which species bind dominantly will depend upon the substrate proteins or the conditions on which the proteins are put.[43] This may, in part, account for the discrepancy between the present results from proteins in solution and the results from those in the crystalline state.[61] The conformations of these motors return to the nucleotide-free state after the release of ADP with a small swing of the LBD in the reverse directions, possibly by further cleft closure of a motor core domain.[29,30] This supports evidence that the force-producing motion takes place in two steps, the first step associated with Pi release and the second associated with ADP release.

It is worthwhile mentioning the population of myosin intermediate species during the steady state of ATP hydrolysis. According to Bagshaw and Trentham[41] and Taylor,[62] in the case of MII, the composition of the steady-state complexes comprises ~87% M**.ADP.Pi, >~9% M*.ATP, and ~4% $M^{\dagger}$.ADP at 21 °C and pH 8.0. If we assume that the overall kinetic processes are common to all myosins and that S1*.ATP and S1**.ADP.Pi of the two processive myosins have almost the same conformation, >~96% of the steady-state complexes would have S1**.ADP.Pi-like conformations. For this situation, we chose this temperature and pH close to 8.0 in the present study. On the other hand, there is evidence that the same ligand binding could induce multiple conformations of myosin, coexisting in equilibrium, whose relative populations are influenced by both temperature and nature of the bound ligand.[61,63] Indeed, it appears that the AMPPNP- and ADP.BeF_3^-[X]-bound states comprise a mixture of two states, M**.ADP.Pi and nucleotide-free states in comparable proportions at 20 °C from the fluorescence intensity changes.[63] The measured scattering profile cannot distinguish between a solution containing a single conformer or multiple conformers and represents a weighted average over profiles for the conformers present in solution. However, the SAXS profiles of MV-S1IQ2 and MVI-S1 with AMPPNP bound closely resembled those in the ADP.Pi-bound state or transition analog-bound states. Thus, the local structural differences that determine the kinetics of nucleotide

Please cite this article as: Sugimoto, Y., et al., Reverse Conformational Changes of the Light Chain-binding Domain of Myosin V and VI Processive Motor Heads During and After a Hydrolysis of ATP..., J Mol Biol (2009), doi:10.1016/j.jmb.2009.07.013

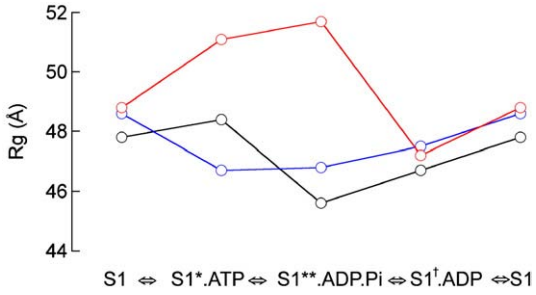

Fig. 9. Reconciling radii gyration (R_g) with the reaction steps of ATPase cycle of S1. The blue circle denotes MV-S1IQ2, the red circle denotes MVI-S1, and the black circle denotes MII-S1 (as a reference). The data were taken from Table 1.

binding are too small to be discerned by SAXS and/or these nucleotides produce different distributions of states.

In SAXS experiments with S1, the change in R_g is dominated by the magnitude of the lever-arm motion, and in Fig. 9, the R_g values in Table 1 are reconciled with the reaction steps of ATPase cycle of S1 to show an opposite change in the LBD of the MV-S1IQ2 and MVI-S1 constructs. It is clear that major rearrangements of the LBD occur upon ATP binding to and releasing Pi or ADP from S1. The net displacement would be the difference between the positions of the LBD in the transition state and the stable ADP-dissociated state. The results strongly suggest that the conformational changes of the LBD as the ATP-driven lever action are responsible for motility, consistent with the view provided by three-dimensional reconstruction images of the actin-bound myosin V and VI constructs showing that the distal portion of S1 oriented in the opposite direction to each other.[24,30] As seen in Fig. 9, the amount of R_g change of MVI-S1 in the Pi release step is ~6.4 times as large as that of MV-S1IQ2, revealing the most compact conformation in the ADP-bound state, which is, in fact, very similar in R_g to the MV-S1IQ2 ADP-bound state. Its modeling was also made, and the optimal atomic structural model is shown in Fig. 8c (see below), suggesting that the large stroke of MVI-S1 during translocation on actin is associated with a greater angular movement of its LBD upon Pi release.

Pre- and post-powerstroke orientations of the LBD of MV-S1IQ2 and MVI-S1

Primed (pre-powerstroke) and re-primed (post-powerstroke) conformations of the MV-S1IQ2 and MVI-S1 constructs were examined by the construction of atomic structural models.

In the case of MV-S1IQ2, the initial atomic structural model yielded a moderate match to the SAXS-derived molecular envelope in the nucleotide-free state (Fig. 7a), and the model for the protein in the presence of ATP was obtained by bending the LBD of the nucleotide-free model by ~50°, the change being comparable to that occurring in MII-S1 with the addition of ATP. In contrast, for MVI-S1, the initial atomic structural model did not fit to the SAXS-derived molecular envelope in the nucleotide-free state but yielded a better match by reducing the bending angle of the LBD by ~50° (Fig. 8c). Thus, MVI-S1 in solution has a much less bent structure than the post-transition model predicted from the reported crystal structures. The atomic structural model yielded a good match to the SAXS-derived envelope in ATP solution. In Figs. 7c and 8c, the primed and re-primed orientations of the LBD of the MV-S1IQ2 and MVI-S1 models, respectively, are compared. The difference (~50°) in the angle between the α-helical backbones of the LBD of MV-S1IQ2 was smaller than the ~70° change, which was estimated by single-molecule fluorescence polarization[11,64] and was comparable to that of MII-S1 previously estimated by SAXS[33–35] as well as the results presented in the present work. Although the motion of the LBD within the molecule was complicated, the corresponding angular change between the LBDs in the two MVI-S1 models was ~100°, which was much less than the ~180° predicted from their crystal structure models to allow a maximal working stroke length (~12nm or ~18nm).[31] As mentioned above, the largest R_g change of the MVI-S1 construct was observed in the release step of Pi (Fig. 9). Our modeling suggests that an angular change of the LBD occurring upon the release of Pi (that is, in the transition to an ADP-bound state) is ~130°. If the crystal conformation of MVI-S1 in the nucleotide-free state represents the conformation of the actin-bound state (the rigor-like state),[24,30] in our modeling the LBD may bend further by ~30° upon the release of ADP on actin. If an ~180° swing is required to allow a maximal stride on actin for MVI-S1, there must be additional changes or elements in the conformation of the converter including unwinding[53] or melting in the head/neck region as in kinesin.[65] Recent polarized total reflection fluorescence studies on MVI have suggested that in addition to a flexible tail domain, there is a compliant element between the motor core domain and the LBD to allow a large Brownian motion of the LBD.[19] These would make it possible for MVI to accommodate variable step sizes along the actin filament in the processive transition, whereas the motion of MV-S1 with a tightly distributed, large step size may be rectified by its long and relatively stiff neck with six IQ motifs.[7,9]

The discrepancy between the processive step size of a two-headed construct and the working stroke of a single-headed construct on actin in MV and MVI is explained by the fact that a processive step consists of a working stroke of the attached head and a Brownian search of the unbound head for the next binding site.[12,14,16,18,31,53]

Comparisons of partial crystal structures in various analog states have revealed that nucleotide binding, hydrolysis, and product release all correlate to small movements within the motor core domain and these movements are transmitted through rearrangements of the converter domain to the LBD.[29,31] Consistent with this, our SAXS results indicate that the isomerization, ATP hydrolysis, Pi release, and ADP release are accompanied

Please cite this article as: Sugimoto, Y., et al., Reverse Conformational Changes of the Light Chain-binding Domain of Myosin V and VI Processive Motor Heads During and After a Hydrolysis of ATP..., J Mol Biol (2009), doi:10.1016/j.jmb.2009.07.013

by global conformational changes in the head domain. Although the stereo-specific interaction of the large insert 2 and the converter domain of MVI[30,31,66] may be predominantly related to the directionality reversal, whether the elements determining such a directional preference in processive myosin motors reside in reverse directions of the conformational change of the LBD[7,13,67] or that within the motor core domain[14,66,68] or both of them[27,30,31] is still under investigation. The present SAXS results underscored the ATP-powered, directed lever action of the LBD for the directional preference.

Conclusion

Using the SAXS techniques under physiological conditions, we demonstrated that the LBDs of myosin VI-S1 during hydrolysis of ATP and in ADP-bound or nucleotide-free state are positioned completely opposite to those of myosin V-S1 or myosin II-S1, suggesting that the directed motion of myosins V and VI along the actin filament is associated with directional alterations of the LBD within the S1 domain during an ATPase cycle. The primed conformations in the transition (pre-power-stroke) state in these myosin S1s were produced upon binding of ATP, and the processive transition was generated by re-priming of their conformational changes upon the phosphate (Pi) or ADP release from the ADP and Pi-bound state. The much larger change in the radius of gyration for MVI-S1 with the release of Pi is associated with the production of the large stroke size of this motor during processive translocation on actin. The comparison between the transition and post-transition atomic structural models based upon the SAXS-derived shape envelopes revealed that the angular change between the LBDs was ~50° for MV-S1IQ2 and ~100° or ~130° for MVI-S1, inferring that the ADP/Pi-bound MV-S1IQ2 and nucleotide-free MVI-S1 in solution assume a less bent conformation of their LBD than in crystal or in the actin-bound form. For MVI-S1, some additional changes or elements of the motor domain are needed to perform its maximal stroke length on actin. The SAXS results indicated that the conformational changes of the LBD as the lever action play a critical role in ATP-driven motility.

Materials and Methods

Generation of the expression vectors for myosin V and VI constructs

Mouse myosin Va cDNA clones containing nucleotides −35 to 1549 and 1549 to 3928 in pBluescript were supplied by Dr. N. Jenkins of the National Cancer Institute, National Institutes of Health (USA). Myosin Va with two IQ motifs (MV-S1IQ2, nucleotides 1–2468) containing myc and hexa-histidine tag sequences in pBlueBac4His baculovirus transfer vector (Invitrogen) was made as described previously.[37,69] The MV-S1IQ2 cDNA fragment obtained by NheI-KpnI digestion was recombined with pFastBac1 baculovirus transfer vector (Invitrogen) at the polylinker region. This construct contains the amino acid residues Met1-Gln822 of myosin Va. Mouse myosin VI cDNA clones containing nucleotides −150 to 2565 and 1460 to 3708 in pBluescript were provided by Dr. K. Avraham of Tel Aviv University (Israel). A cDNA fragment of myosin VI (nucleotides 1–3156) was made by KpnI-PflMI digestion, followed by ligation as described previously.[36,38] A unique NheI site at the 5′ side of the initiation codon and a new KpnI site at the 5′ side of the inherent KpnI were created to produce a cDNA fragment of myosin VI-S1, and then the cDNA cut by NheI-KpnI digestion was inserted into pFastBac1 at the polylinker region. A hexa-histidine tag sequence with a stop codon was introduced at the 3′ side of the KpnI site. This construct contains the amino acid residues Met1-Glu924 of myosin VI-S1, in which a longer tail was necessary to obtain a stable construct.

Preparation of recombinant myosins V-S1IQ2 and VI-S1

Recombinant myosins V-S1IQ2 and VI-S1 were obtained from Sf9 cells using the baculovirus expression system. Sf9 cells (about 2×10^{10}) were co-infected with heavy chain and calmodulin viruses and cultured at 28 °C for 3 days. The cells were homogenized by sonication in a lysis buffer [0.1 M NaCl, 30 mM Tris–HCl (pH 8.0), 2 mM $MgCl_2$, 0.2 mM ethylene glycol bis(β-aminoethyl ether)*N*,*N*′-tetraacetic acid (EGTA), 1 mM ATP, 1 mM DTT, and 5 μg/ml leupeptin]. After centrifugation at 140,000*g* for 30 min, myosin was subjected to Ni^{2+}-NTA agarose (Qiagen, Hilden, Germany) columns. After wash with a 40-fold resin volume of buffer A (0.3 M NaCl, 0.1 mM EGTA, 1 mM DTT, and 1 μg/ml leupeptin) containing 10 mM imidazole–HCl (pH 7.5), myosin was eluted with buffer A containing 0.2 M imidazole–HCl (pH 7.5). The fractions containing myosin were pooled, and the protein was concentrated with a VIVASPIN concentrator (Vivascience, Carlsbad, CA) to ~10 mg/ml. Myosin was then purified by gel filtration on a Sephacryl S-300 HR column (2.6 cm × 65 cm) equilibrated with 0.3 M KCl, 20 mM Tris–HCl (pH 7.5), 1 mM ethylenediaminetetraacetic acid, and 0.5 mM DTT. Purified protein (20–50 mg) was obtained from 40 ml pellet of the Sf9 cells. Purified myosin S1s were stored on ice and used within 2 days.

Preparation of skeletal myosin II-S1

Myosin II molecules prepared from chicken skeletal (breast) muscle were digested by papain to obtain S1s according to the method of Margossian and Lowey.[70] The ATPase activity of MII-S1 was measured at 25 °C in a reaction mixture containing 0.5 M KCl, 30 mM Tris–HCl (pH 7.5), 1 μM S1, 5 mM $MgCl_2$ ($CaCl_2$ or ethylenediaminetetraacetic acid), and 2 mM ATP. After the reaction was stopped, the inorganic phosphate released was measured by the method of Youngburg and Youngburg.[71]

Other procedures

SDS-PAGE was carried out on a 5–15% polyacrylamide gradient slab gel using a discontinuous buffer system (see Fig. 1b). The gels were stained for protein with Coomassie Brilliant Blue. Molecular mass markers used were myosin

Please cite this article as: Sugimoto, Y., et al., Reverse Conformational Changes of the Light Chain-binding Domain of Myosin V and VI Processive Motor Heads During and After a Hydrolysis of ATP..., J Mol Biol (2009), doi:10.1016/j.jmb.2009.07.013

heavy chain (205 kDa), β-galactosidase (116 kDa), phosphorylase b (97.4 kDa), bovine serum albumin (BSA) (66 kDa), ovalbumin (45 kDa), and carbonic anhydrase (29 kDa).

The protein concentrations of all myosin S1s were determined by the micro Biuret method using BSA as a standard.

SAXS experiments

SAXS measurements were performed with the use of a monochromatized synchrotron X-ray beam (wavelength, 1.50 Å). Synchrotron radiation from a bending magnet source in the positron storage ring at the Photon Factory (KEK), Tsukuba, Japan, operated at 2.5 GeV with a ring current between 350 and 450 mA was selected and collimated with the double focusing optics installed at beamline 15A1.[39,40] In order to allow small-angle measurements required for the present experiments, we used a beam of dimensions 0.20 mm (vertical) × 0.20 mm (horizontal) at the detector plane with a specimen-to-detector distance of 2.42 m. The higher-angle scattering data were measured with a camera length of 1.02 m. Scattered X-rays were recorded by a linear position-sensitive detector with a spatial resolution of ca 0.3 mm (Rigaku Denki, Tokyo, Japan). The beam intensity incident at the specimen was monitored with an ion chamber placed in front of the specimen. Each purified S1 was used immediately after it came off an HPLC gel-filtration column for the X-ray experiments. The sample was inserted in a temperature-controlled cell with two mica windows through which X-rays passed, and the temperature was maintained at 20 °C. Protein concentration, c, was varied from 2 to 8 mg/ml. Normally, five measurements for each myosin S1 preparation were done at different concentrations. Depending upon the beam current, the exposure time of X-rays was varied but was always less than 90 s to minimize radiation damage of the samples. Buffer scattering measurements were performed periodically throughout the measurement sequence. After correction for the variations in the beam intensity, as measured by the current values from the ion chamber, we obtained net intensity data, $I(Q,c)$, by subtracting the buffer scattering from the sample solution scattering, where Q is the momentum transfer vector ($=4\pi\sin\theta/\lambda$, in which 2θ and λ are the scattering angle and the wavelength of the monochromatized X-rays used, respectively) and c is the protein concentration. The composition of the buffer solution used for MV-S1IQ2 and MVI-S1 was 150 mM KCl, 20 mM Tris–HCl (pH 7.5), 1 mM DTT, 2 μg/ml leupeptin, 1 mM EGTA, and 0.1 mM $CaCl_2$. The buffer solution of MII-S1 contained 120 mM NaCl, 30 mM Tris–HCl (pH 7.5), and 1 mM DTT. MgATP or MgADP was added to the protein solution to a final concentration of 2 mM. The protein concentration of myosin S1 samples used for X-ray experiments was determined by the micro Biuret method using BSA as a standard.

Analysis of SAXS intensity data

The apparent radius of gyration, $R_g(c)$, was determined from the slope of the Guinier plot of the SAXS data in the narrow Q range where the Guinier's criterion ($Q=1/R_g$)[42] is involved. The final R_g values at zero protein concentration were determined by means of a variance-weighted least-squares fit to the data points at various protein concentrations (c). The $I(0,c)$ value was evaluated by extrapolating the Guinier plot to $Q=0$ for each c. The extrapolated intensity data were used to generate the unobserved data in the small-angle region. The $I(Q,c)/c$ data were extrapolated to $c=0$ at each Q and the extrapolated values were averaged, and the intensity profiles of $I(Q,0)$ obtained were spliced to those measured at the short camera length and at high protein concentrations by means of the least-squares fit to obtain the wide-range intensity data of $0 \le Q \le 0.240$ Å^{-1}. The pair-distance distribution function, $p(r)$, was calculated by an indirect Fourier transformation[42,45] of the $I(Q,0)$ data over the entire observed Q range. The slightly oscillatory nature in $p(r)$ was due to the termination effect of Fourier integration. The maximum chord length, D_{max}, of the molecule was determined as the distance at which the $p(r)$ function eventually drops to zero.

Ab initio reconstruction of molecular shape envelopes

The program DAMMIN[46] was used to construct three-dimensional molecular envelopes that fit to the SAXS data. Reconstruction was conducted as follows. A protein shape was first expressed by a face-centered cubic spherical ball-filling model in a volume confined by D_{max} of $p(r)$ functions and was then optimized with a compactness criterion by removing and/or adding balls in appropriate places. Simulated annealing procedure was used to fit the observed X-ray scattering intensity curves. A number of independent repeat runs were performed for each reconstruction. The obtained models were sorted and averaged, and the most probable model including corrections both for contrast and hydration with solvent for each case was researched starting from the average structure.

Construction of the atomic structural models of the MV-S1IQ2 and MVI-S1 constructs

In modeling the MV-S1IQ2 construct in the nucleotide-free state, the crystal structure of the LBD portion of MV-S1 (PDB ID: 2IX7[47]) with the calmodulin molecule bound to the two IQ motifs was combined to the crystal structure consisting of the motor core domain and an IQ1 portion (PBD ID: IOE9[28]) by superimposing their IQ motifs together with bound myosin light chain and calmodulin. The alignment for both crystal structures was performed with the PyMOL molecular graphics system.[49] The atomic structural model of the MVI-S1 construct in the nucleotide-free state was constructed by using the partial crystal structure of MV1-S1IQ1 (PDB ID: 2BKI[30]) and the LBD crystal structure of MV-S1 (PDB ID: 2IX7). A structural alignment was performed between the IQ motifs with bound calmodulin molecules in both crystal structures, and two crystal structures were then combined with each other to obtain a complete atomic structural model. The atomic structural model of the MVI-S1 construct in the presence of ATP was constructed by using the partial crystal structure of MV1-S1 (PDB ID: 2V26[31]) including the residues until the proximal helix of insert 2 and with ADP and Vi bound to the nucleotide binding sites in the motor core domain and the LBD crystal structure of MV-S1 (PDB ID: 2IX7). Firstly, the crystal structures of 2V26 and 2BKI were aligned to obtain the crystal structural model including an insert 2-IQ motif with bound calmodulin molecules. Next, the LBD crystal structure of 2IX7 was aligned and then combined to the distal part of the crystal structure of 2V26 to obtain a complete atomic structural model in the transition state.

The goodness of fit of the final model was examined by calculating the following R-factor between the observed

Please cite this article as: Sugimoto, Y., et al., Reverse Conformational Changes of the Light Chain-binding Domain of Myosin V and VI Processive Motor Heads During and After a Hydrolysis of ATP..., J Mol Biol (2009), doi:10.1016/j.jmb.2009.07.013

intensity data [$I_{obs}(Q)$] and those [$I_{calc}(Q)$] calculated from the model.

$$R = \sum_i Q_i^2 \{I_{obs}(Q_i) - I_{calc}(Q_i)\}^2 / \sum_i Q_i^2 I_{obs}(Q_i).$$

The final optimal models in the minimal R-value range were determined by further examining the goodness of fit with the SAXS molecular envelope and the overall agreement between the calculated and observed intensity profiles.

Acknowledgements

The authors thank the members of Soka University for their help in the sample preparation and Y. Takezawa of Osaka University for his expert help in X-ray experiments at the Photon Factory. Thanks are also due to Tom Irving of Illinois Institute of Technology for critical reading of the manuscript and discussion. This work was supported in part by Special Coordination Funds from the Ministry of Education, Science, Sports, and Culture of Japan (to K. W.) and National Institute of Health Grants 048526 and AR41653 (to M.I.). The SAXS experiments on myosin V-S1 and VI-S1 constructs have been approved by the Photon Factory Advisory Committee (No. 2003G143 and No. 2005G143).

References

1. Sellers, J. R. (2000). Myosin: a diverse superfamily. *Biochim. Biophys. Acta*, **1496**, 3–22.
2. Moosker, M. S. & Cheney, R. E. (1995). Unconventional myosin. *Annu. Rev. Cell Dev. Biol.* **11**, 633–675.
3. Mehta, A. D., Rock, R. S., Rief, M., Spudich, J. A., Mooseker, M. S. & Cheney, R. E. (1999). Myosin-V is a processive actin-based motor. *Nature*, **400**, 590–593.
4. Walker, M. L., Burgess, S. A., Sellers, J. R., Wang, F., Hammer, J. A., III, Trinick, J. & Knight, J. (2000). Two-headed binding of a processive myosin to F-actin. *Nature*, **405**, 804–807.
5. Rief, M., Rock, R. S., Mehta, A. D., Mooseker, M. S., Cheney, R. E. & Spudich, J. A. (2002). Myosin-V stepping kinetics: a molecular model for processivity. *Proc. Natl Acad. Sci. USA*, **97**, 9482–9486.
6. Cappello, G., Pierobon, P., Symonds, C., Busoni, L., Gebhardt, J. C. M., Rief, M. & Prost, J. (2007). Myosin V stepping mechanism. *Proc. Natl Acad. Sci. USA*, **25**, 15328–15333.
7. Purcell, T. J., Morris, C. A., Spudich, J. A. & Sweeney, H. J. (2002). Role of the lever arm in the processive stepping of myosin V. *Proc. Natl Acad. Sci. USA*, **99**, 14159–14164.
8. Tanaka, H., Homma, K., Iwane, A.-H., Katayama, E., Ikebe, R., Saito, J. *et al.* (2002). The motor domain determines the large step of myosin-V. *Nature*, **415**, 192–195.
9. Sakamoto, T., Wang, F., Schmitz, S., Xu, Y., Xu, Q., Molloy, J. E. *et al.* (2003). Neck length and processivity of myosin V. *J. Biol. Chem.* **278**, 29201–29207.
10. Sakamoto, T., Amitani, I., Yokota, E. & Ando, T. (2000). Direct observation of processive movement by individual myosin molecules. *Biochem. Biophys. Res. Commun.* **272**, 586–590.
11. Forkey, J. N., Quinlan, M. E., Shaw, M. A., Corrie, J. E. T. & Goldman, Y. E. (2003). Three-dimensional structural dynamics of myosin V by single-molecule fluorescence polarization. *Nature*, **422**, 399–404.
12. Shiroguchi, K. & Kinosita, K., Jr (2007). Myosin V walks by lever action and Brownian motion. *Science*, **316**, 1208–1212.
13. Rock, R. S., Rice, S. E., Wells, A. L., Purcell, T. J., Spudich, J. A. & Sweeney, H. L. (2001). Myosin VI is a processive backward motor with a large step size. *Proc. Natl Acad. Sci. USA*, **98**, 13655–13659.
14. Nishikawa, S., Homma, K., Komori, Y., Iwaki, M., Wazawa, T., Iwane, A.-H. *et al.* (2002). Class VI myosin moves processively along actin filaments backward with large steps. *Biochem. Biophys. Res. Commun.* **290**, 311–317.
15. Buss, F., Spudich, G. & Kendrick-Jones, J. (2004). Myosin VI: cellular functions and motor properties. *Annu. Rev. Cell Biol.* **20**, 649–675.
16. Ali, M. Y., Homma, K., Iwane, A.-H., Adachi, K., Itoh, H., Kinosita, K., Jr *et al.* (2004). Unconstrained steps of myosin VI appear longest among known molecular motors. *Biophys. J.* **86**, 3804–3810.
17. Lister, I., Schmitz, S., Walker, M., Trinick, J., Buss, F., Veigel, C. & Kendrick-Jones, J. (2004). A monomeric myosin VI with a large working stroke. *EMBO J.* **23**, 1729–1738.
18. Lan, G. & Sun, S. X. (2006). Flexible light chain and helical structure of F-actin explain the movement and step size of myosin-VI. *Biophys. J.* **97**, 4002–4013.
19. Sun, Y., Schroeder, H. W., III, Beausang, J. F., Homma, K., Ikebe, M. & Goldman, Y. E. (2007). Myosin VI walks "wiggly" on actin with large and variable tilting. *Mol. Cell*, **28**, 954–964.
20. Morris, C. A., Wells, A. L., Yang, Z., Chen, L.-Q., Baldacchino, C. V. & Sweeney, H. L. (2003). Calcium functionally uncouples the heads of myosin VI. *J. Biol. Chem.* **278**, 23324–23330.
21. Park, H., Ramamurthy, B., Travaglia, M., Safer, D., Chen, L.-Q., Franzini-Armstrong, C. *et al.* (2006). Full-length myosin VI dimerizes and moves processively along actin filaments upon monomer clustering. *Mol. Cell*, **21**, 331–336.
22. Buss, F. & Kendrick-Jones, J. (2008). How are the cellular functions of myosin VI regulated within cell? *Biochem. Biophys. Res. Commun.* **369**, 165–175.
23. Bahloul, A., Chevreux, G., Wells, A. L., Martin, D., Noit, J., Yang, Z. *et al.* (2004). The unique insert in myosin VI is a structural calcium-calmodulin binding site. *Proc. Natl Acad. Sci. USA*, **101**, 4787–4792.
24. Wells, A. L., Lin, A. W., Chen, L.-Q., Safer, D., Cain, S. M., Hasson, T. *et al.* (1999). Myosin VI is an actin-based motor that moves backwards. *Nature*, **401**, 505–508.
25. Altmann, D., Sweeney, H. L. & Spudich, J. A. (2004). The mechanism of myosin VI translocation and its load-induced anchoring. *Cell*, **116**, 737–746.
26. Cramer, P. (2000). Myosin VI: roles for a minus-end directed actin motor in cells. *J. Cell Biol.* **150**, F121–F126.
27. Bryant, Z., Altmann, D. & Spudich, J. A. (2007). The power stroke of myosin VI and the basis of reverse directionality. *Proc. Natl Acad. Sci. USA*, **104**, 772–777.
28. Coureux, P.-D., Wells, A. L., Ménétrey, J., Yengo, C. M., Morris, C. A., Sweeney, H. L. & Houdusse, A. (2003). A structural state of the myosin V motor without bound nucleotide. *Nature*, **425**, 419–423.

Please cite this article as: Sugimoto, Y., et al., Reverse Conformational Changes of the Light Chain-binding Domain of Myosin V and VI Processive Motor Heads During and After a Hydrolysis of ATP..., J Mol Biol (2009), doi:10.1016/j.jmb.2009.07.013

29. Coureux, P.-D., Sweeney, H. L. & Houdusse, A. (2004). Three myosin V structures delineate essential features of chemo-mechanical transduction. *EMBO J.* **23**, 4527–4537.
30. Ménétrey, J., Bahloul, A., Wells, A. L., Yengo, C. M., Morris, C. A., Sweeney, H. L. & Houdusse, A. (2005). The structure of the myosin VI motor reveals the mechanism of directionality reversal. *Nature*, **435**, 779–785.
31. Ménétrey, J., Linas, P., Mukherjea, M., Sweeney, H. L. & Houdusse, A. (2007). The structural basis for the large powerstroke of myosin VI. *Cell*, **131**, 300–308.
32. Ménétrey, J., Linas, P., Cicolari, J., Squires, G., Liu, X., Li, A. *et al.* (2008). The post-rigor structure of myosin VI and implication for the recovery stroke. *EMBO J.* **27**, 244–252.
33. Wakabayashi, K., Tokunaga, M., Kohno, I., Sugimoto, Y., Hamanaka, T., Takezawa, Y. *et al.* (1992). Small-angle synchrotron X-ray scattering reveals distinct shape changes of the myosin head during hydrolysis of ATP. *Science*, **258**, 443–447.
34. Sugimoto, Y., Tokunaga, M., Takezawa, Y., Ikebe, M. & Wakabayashi, K. (1994). Conformational changes of the myosin heads during hydrolysis of ATP analyzed by X-ray solution scattering. *Biophys. J.* **68**, 29s–34s.
35. Mendelson, R. A., Schneider, D. K. & Stone, D. B. (1996). Conformations of myosin subfragment 1 ATPase intermediates from neutron and X-ray scattering. *J. Mol. Biol.* **256**, 1–7.
36. Sato, O., White, H. D., Inoue, A., Belknap, B., Ikebe, R. & Ikebe, M. (2004). Human deafness mutation of myosin VI (C442Y) accelerates the ADP dissociation rate. *J. Biol. Chem.* **279**, 28844–28854.
37. Homma, K., Saito, J., Ikebe, R. & Ikebe, M. (2000). Ca^{2+}-dependent regulation of the motor activity of myosin V. *J. Biol. Chem.* **275**, 34766–34771.
38. Yoshimura, M., Homma, K., Saito, J., Inoue, A., Ikebe, R. & Ikebe, M. (2001). Dual regulation of mammalian myosin VI motor function. *J. Biol. Chem.* **276**, 39600–39607.
39. Amemiya, Y., Wakabayashi, K., Hamanaka, T., Wakabayashi, T., Matsushita, T. & Hashizume, H. (1983). Design of a small-angle diffractometer using synchrotron radiation at the Photon Factory. *Nucl. Instrum. Methods*, **208**, 471–477.
40. Amemiya, Y., Wakabayashi, K. & Itoh, K. (1998). Renewal of the mirror system in the BL15A1 optics. *Photon Fact. News*, **16**, 9–10.
41. Bagshaw, C. & Trentham, D. R. (1974). The characterization of myosin-product complexes and of product-release steps during the magnesium ion-dependent adenosine-triphosphate reactions. *Biochem. J.* **141**, 331–349.
42. Glatter, O. (1981). In (Glatter, O. & Kratky, O., eds), , chapt. 4 and 5 Academic Press, New York, NY.
43. Henry, G. D., Maruta, S., Ikebe, M. & Sykes, B. D. (1993). Observation of multiple myosin subfragment 1-ADP-fluoroberyllate complexes by ^{19}F NMR spectroscopy. *Biochemistry*, **32**, 10451–10456.
44. Bagshaw, C. R. (1993). *Muscle Contraction*, chapt. 5 Chapman & Hall, London, UK.
45. Svergun, D. I. (1992). Determination of the regularization parameter in indirect-transform methods using perceptual criteria. *J. Appl. Crystallogr.* **25**, 495–503.
46. Svergun, D. I. (1999). Restoring low resolution structure of biological macromolecules from solution scattering using simulated annealing. *Biophys. J.* **76**, 2879–2886.
47. Svergun, D. I. (2000). Advanced solution scattering data analysis methods and their application. *J. Appl. Crystallogr.* **33**, 530–534.
48. Terrak, M., Rebowski, G., Lu, R. C., Grabarek, Z. & Dominguez, R. (2005). Structure of the light chain-binding domain of myosin V. *Proc. Natl Acad. Sci. USA*, **102**, 12718–12723.
49. The PyMol Molecular Graphic System [http://www.pymol.source forge.net/].
50. Kozin, M. B. & Svergun, D. I. (2000). A software system for rigid-body modeling of solution scattering data. *J. Appl. Crystallogr.* **33**, 575–577.
51. Hirai, M., Iwase, H., Hayakawa, T., Miura, K. & Inoue, K. (2002). Structural hierarchy of several proteins observed by wide-angle solution scattering. *J. Synchrotron Radiat.* **9**, 202–205.
52. Spink, B. J., Sivaramakrishnan, S., Lipfelt, J., Doniach, S. & Spudich, J. A. (2008). Long α-helical tail domains bridge the gap between structure and function of myosin VI. *Nat. Struct. Mol. Biol.* **15**, 591–597.
53. Rock, R. S., Ramamurthy, B., Dunn, A. R., Beccafico, S., Rami, B. R., Morris, C. A. *et al.* (2005). A flexible domain is essential for the large step size and processivity of myosin VI. *Mol. Cell*, **17**, 603–609.
54. De La Cruz, E. M., Wells, A. L., Rosenfeld, S. S., Ostap, E. M. & Sweeney, H. L. (1999). The kinetic mechanism of myosin V. *Proc. Natl Acad. Sci. USA*, **96**, 13726–13731.
55. Robblee, J. P., Cao, W., Henn, A., Hannemann, D. E. & De La Cruz, E. M. (2005). Thermodynamics of nucleotide binding to actomyosin V and VI: a positive heat capacity change accompanies strong ADP binding. *Biochemistry*, **279**, 2333–2336.
56. De La Cruz, E. M., Ostap, E. M. & Sweeney, H. L. (2001). . Kinetic mechanism and regulation of myosin VI. *J. Biol. Chem.* **276**, 32373–32381.
57. Robblee, J. P., Olivales, A. O. & De La Cruz, E. M. (2004). Mechanism of nucleotide binding to actomyosin VI. *J. Biol. Chem.* **279**, 38608–38617.
58. Nyitrai, M. & Geeves, M. A. (2009). Adenosine diphosphate and strain sensitivity in myosin motors. *Philos. Trans. R. Soc. London*, **B359**, 1867–1877.
59. Yengo, C. M., De La Cruz, E. M., Safer, D., Ostap, E. M. & Sweeney, H. L. (2002). Kinetic characterization of the weak binding states of myosin V. *Biochemistry*, **41**, 8508–8517.
60. Enfres, N. F., Yoshioka, C., Milligan, R. A. & Vale, R. D. (2006). A lever-arm rotation drives motility of the minus-end-directed kinesin NCD. *Nature*, **436**, 875–876.
61. Maruta, S., Uyehara, Y., Aihra, T. & Katayama, E. (2004). Interaction of myosin. ADP–fluorometal complexes with fluorescent probes and direct observation using quick-freeze deep-etch electron microscopy. *J. Biochem. (Tokyo)*, **136**, 57–64.
62. Taylor, E. W. (1977). Transient phase of adenosine triphosphate hydrolysis by myosin heavy meromyosin, and subfragment 1. *Biochemistry*, **16**, 732–740.
63. Málnási-Csizmadia, A., Pearson, D. S., Kovács, M., Wooley, R. J., Geeves, M. A. & Bagshaw, C. (2001). Kinetic resolution of a conformational transition and the ATP hydrolysis step using relaxation methods with a *Dictyostelium* myosin II mutant containing a single tryptophan residues. *Biochemistry*, **40**, 12727–12737.
64. Shih, W. M., Gryczynski, Z., Lakowicz, J. R. & Spudich, J. A. (2000). A FRET-based sensor reveals large ATP hydrolysis-induced conformational changes and three distinct states of molecular motor myosin. *Cell*, **102**, 683–694.
65. Rice, S., Lin, A. W., Safer, D., Hart, C. L., Naber, N., Carragher, B. O. *et al.* (1999). A structural change in the

Please cite this article as: Sugimoto, Y., et al., Reverse Conformational Changes of the Light Chain-binding Domain of Myosin V and VI Processive Motor Heads During and After a Hydrolysis of ATP..., J Mol Biol (2009), doi:10.1016/j.jmb.2009.07.013

kinesin motor protein that drives motility. *Nature*, **402**, 778–784.
66. Park, H., Li, A., Chen, L.-Q., Houdusse, A., Selvin, P. R. & Sweeney, H. L. (2007). The unique insert at the end of the myosin VI motor is the sole determinant of directionality. *Proc. Natl Acad. Sci. USA*, **104**, 778–783.
67. Tsiavaliaris, G., Fujita-Becker, S. & Manshtein, D. J. (2004). Molecular engineering of a backwards-moving myosin motor. *Nature*, **427**, 558–561.
68. Homma, K., Yoshimura, M., Saito, J., Ikebe, R. & Ikebe, M. (2001). The core of the motor domain determines the direction of myosin movement. *Nature*, **412**, 831–834.
69. O'Rielly, D. R., Miller, L. K. & Luckow, V. A. (1992). *Baculovirus Expression Vectors: A Laboratory Manual.* W. H. Freeman and Co., New York, NY.
70. Margossian, S. S. & Lowey, S. (1982). Preparation of myosin and its subfragments from rabbit skeletal muscle. *Methods Enzymol.* **85B**, 55–71.
71. Youngburg, G. E. & Youngburg, M. V. (1930). A system of blood phosphorus analysis. *J. Lab. Clin. Med.* **16**, 158–166.

Please cite this article as: Sugimoto, Y., et al., Reverse Conformational Changes of the Light Chain-binding Domain of Myosin V and VI Processive Motor Heads During and After a Hydrolysis of ATP..., J Mol Biol (2009), doi:10.1016/j.jmb.2009.07.013